Determination of the parameters of a Skyrme type effective interaction using the simulated annealing approach

B. K. Agrawal, S. Shlomo, and V. Kim Au

Cyclotron Institute, Texas A&M University, College Station, TX 77843, USA

Abstract

We implement for the first time the simulated annealing method (SAM) to the problem of searching for the global minimum in the hyper-surface of the chi-square function which depends on the values of the parameters of a Skyrme type effective nucleon-nucleon interaction. We undertake a realistic case of fitting the values of the Skyrme parameters to an extensive set of experimental data on the ground state properties of many nuclei ranging from normal to exotic ones. The set of experimental data used in our fitting procedure includes the radii for the valence $1d_{5/2}$ and $1f_{7/2}$ neutron orbits in the ^{17}O and ^{41}Ca nuclei, respectively, and the breathing mode energies for several nuclei, in addition to the typically used data on binding energy, charge radii and spin-orbit splitting. We also include in the fit the critical density ρ_{cr} and further constrain the values of the Skyrme parameters by requiring that (i) the quantity $P = 3\rho\frac{dS}{d\rho}$, directly related to the slope of the symmetry energy S, must be positive for densities up to $3\rho_0$ (ii) the enhancement factor κ, associated with the isovector giant dipole resonance, should lie in the range of $0.1 - 0.5$ and (iii) the Landau parameter G'_0 is positive at $\rho = \rho_0$. We provide simple but consistent schemes to account for the center of mass corrections to the binding energy and charge radii.

I. INTRODUCTION

Since the pioneering work of Brink and Vautherin [1], continuous efforts have been made to readjust the parameters of the Skyrme type effective nucleon-nucleon interaction to better reproduce experimental data. Most of the parameters of the Skyrme interactions available in the literature were obtained by fitting the Hartree-Fock (HF) results to experimental data on bulk properties of a few stable closed shell nuclei. Only recently, several families of the Skyrme parameters e.g., SkI1-6, SLy1-10, SKX and SkO [2, 3, 4, 5, 6, 7] were obtained by fitting HF results to the experimental data on the bulk properties of nuclei ranging from the $\beta-$stable nuclei to those near the proton and/or neutron drip lines. In the SKX interaction, to yield appropriately the values for the binding energy differences between mirror nuclei also referred to as the Coulomb displacement energy (CDE), the contribution of the Coulomb exchange term in the HF equations is ignored and the direct Coulomb term is evaluated by replacing the point proton distribution by its charge distribution. However, it has been further shown in Ref. [8] that the SKX interaction is not suitable for studying the properties of neutron stars. Since, for the SKX interaction, the quantity

$$P = 3\rho \frac{dS}{d\rho}, \tag{1}$$

which is directly related to the slope of the symmetry energy coefficient S, becomes negative for nuclear matter densities ρ well below $3\rho_0$ ($\rho_0 = 0.16$ fm^{-3} is the saturation density). On the other hand, the SkI1-6, SLy1-10 and SkO Skyrme interactions are found to be suitable for the study of neutron stars [8]. But, these families of Skyrme interactions significantly underestimate the values of the CDE for mirror nuclei, since the Coulomb exchange term was included. Thus, it is desirable to have a unified interaction which includes the merits of several families of the Skyrme interactions as mentioned above. One can further enhance the applicability of the Skyrme type effective nucleon-nucleon interaction by imposing certain constraints as discussed below.

The aim of this work is twofold. We implement, for the first time, the simulated annealing method (SAM) [9, 10] to fit the values of the Skyrme parameters and develop a more realistic Skyrme type effective interaction. The SAM is an elegant technique for optimization problems of large scale, in particular, where a desired global extremum is hidden among many local extrema. This method has been found to be an extremely useful tool for a wide variety of minimization problems of large non-linear systems in many different areas of science (e.g.,

see Refs. [11, 12, 13]). Very recently [14, 15], the SAM was used to generate some initial trial parameter sets for the point coupling variant of the relativistic mean field model. In the present context, we use the SAM to determine the values of the Skyrme parameters by searching for the global minimum in the hyper-surface of the χ^2 function given as,

$$\chi^2 = \frac{1}{N_d - N_p} \sum_{i=1}^{N_d} \left(\frac{M_i^{exp} - M_i^{th}}{\sigma_i} \right)^2 \tag{2}$$

where, N_d and N_p are the number of experimental data points and the number of fitted parameters, respectively, σ_i is the theoretical error and M_i^{exp} and M_i^{th} are the experimental and the corresponding theoretical values, respectively, for a given observable. The values of χ^2 depends on the Skyrme parameters, since, the M_i^{th} in Eq. (2) is calculated using the HF approach with a Skyrme type effective nucleon-nucleon interaction.

Toward the purpose of obtaining a more realistic parameterization of the Skyrme interaction, we apply the SAM to fit the HF results to an extensive set of experimental data for the binding energy, charge radii, spin-orbit splitting and root mean square (rms) radii of valence neutron orbits. Our data set used in the fit consists of 14 spherical nuclei, namely, ^{16}O, ^{24}O, ^{34}Si, ^{40}Ca, ^{48}Ca, ^{48}Ni, ^{56}Ni, ^{68}Ni, ^{78}Ni, ^{88}Sr, ^{90}Zr, ^{100}Sn, ^{132}Sn and ^{208}Pb. We also include in our fit the experimental data for the breathing mode energies for the ^{90}Zr, ^{116}Sn, ^{144}Sm and ^{208}Pb nuclei. In addition, we include in the fit, the critical density ρ_{cr} which is determined from the stability conditions for the Landau parameters. [16, 17]. We further constrain the values of the Skyrme parameters by requiring that (i) the quantity P must be positive for densities up to $3\rho_0$; a condition imposed by neutron star models [8], (ii) the enhancement factor κ, associated with the Thomas-Reiche-Kuhn (TRK) sum rule for the isovector giant dipole resonance, lies in the range of $0.1 - 0.5$ [3, 18, 19, 20] and (iii) the Landau parameter G_0', crucial for the spin properties of finite nuclei and nuclear matter, should be positive at $\rho = \rho_0$ [20, 21]. We also provide simple but consistent schemes to account appropriately for the CDE and the center of mass corrections to the binding energy and charge radii. In order to check the reliability of the proposed Skyrme interactions for the study of high density matter, we have examined in detail the behavior of the symmetry energy and the nature of the equation of state (EOS) for pure neutron matter at densities relevant for the neutron star models.

We have organized our paper as follows. In Sec. II we briefly outline the form of the Skyrme nucleon-nucleon (NN) effective interaction and the corresponding energy density

functional adopted in the present work. In this section, we also provide a viable strategies for the calculations of CDE and the center of mass corrections to the total binding energy and charge radii. In Sec. III we provide the relations between the Skyrme parameters and the various nuclear matter properties, which we have used to implement the SAM algorithm as described in Sec. IV. The set of the experimental data along with the theoretical errors and the constraints used in the fit to determine the values of the Skyrme parameters are given in Sec. V. In Sec. VI we present our results for the two different fits carried out in this work. Finally, in Sec. VII we summarize our main results and discuss the scope for the further improvement of the present work.

II. SKYRME ENERGY DENSITY FUNCTIONAL

In this work we adopt the following form for the Skyrme type effective nucleon-nucleon interaction [1, 3],

$$
\begin{aligned}
V_{12} &= t_0 \left(1 + x_0 P_{12}^\sigma\right) \delta(\mathbf{r}_1 - \mathbf{r}_2) \\
&+ \frac{1}{2} t_1 \left(1 + x_1 P_{12}^\sigma\right) \times \left[\overleftarrow{k}_{12}^2 \delta(\mathbf{r}_1 - \mathbf{r}_2) + \delta(\mathbf{r}_1 - \mathbf{r}_2) \overrightarrow{k}_{12}^2\right] \\
&+ t_2 \left(1 + x_2 P_{12}^\sigma\right) \overleftarrow{k}_{12} \delta(\mathbf{r}_1 - \mathbf{r}_2) \overrightarrow{k}_{12} \\
&+ \frac{1}{6} t_3 \left(1 + x_3 P_{12}^\sigma\right) \rho^\alpha \left(\frac{\mathbf{r}_1 + \mathbf{r}_2}{2}\right) \delta(\mathbf{r}_1 - \mathbf{r}_2) \\
&+ i W_0 \overleftarrow{k}_{12} \delta(\mathbf{r}_1 - \mathbf{r}_2)(\overrightarrow{\sigma_1} + \overrightarrow{\sigma_2}) \times \overrightarrow{k}_{12}
\end{aligned}
\tag{3}
$$

where, t_i, x_i, α and W_0 are the parameters of the interaction and P_{12}^σ is the spin exchange operator, $\overrightarrow{\sigma}_i$ is the Pauli spin operator, $\overrightarrow{k}_{12} = -i(\overrightarrow{\nabla}_1 - \overrightarrow{\nabla}_2)/2$ and $\overleftarrow{k}_{12} = -i(\overleftarrow{\nabla}_1 - \overleftarrow{\nabla}_2)/2$. Here, the right and left arrows indicate that the momentum operators act on the right and on the left, respectively. The corresponding mean-field V_{HF} and the total energy E of the system are given by,

$$
V_{HF} = \frac{\delta \mathcal{H}}{\delta \rho}, \qquad E = \int \mathcal{H}(r) d^3 r
\tag{4}
$$

where, the Skyrme energy density functional $\mathcal{H}(r)$, obtained using Eq. (3), is given by [1, 3],

$$
\mathcal{H} = \mathcal{K} + \mathcal{H}_0 + \mathcal{H}_3 + \mathcal{H}_{\text{eff}} + \mathcal{H}_{\text{fin}} + \mathcal{H}_{\text{so}} + \mathcal{H}_{\text{sg}} + \mathcal{H}_{\text{Coul}}
\tag{5}
$$

where, $\mathcal{K} = \frac{\hbar^2}{2m} \tau$ is the kinetic energy term, $\mathcal{H}_0$ is the zero-range term, $\mathcal{H}_3$ the density dependent term, $\mathcal{H}_{\text{eff}}$ an effective-mass term, $\mathcal{H}_{\text{fin}}$ a finite-range term, $\mathcal{H}_{\text{so}}$ a spin-orbit term,

$\mathcal{H}_{sg}$ a term due to tensor coupling with spin and gradient and $\mathcal{H}_{Coul}$ is the contribution to the energy density due to the Coulomb interaction. For the Skyrme interaction of Eq. (3), we have,

$$\mathcal{H}_0 = \frac{1}{4}t_0 \left[(2+x_0)\rho^2 - (2x_0+1)(\rho_p^2 + \rho_n^2) \right], \tag{6}$$

$$\mathcal{H}_3 = \frac{1}{24}t_3\rho^\alpha \left[(2+x_3)\rho^2 - (2x_3+1)(\rho_p^2 + \rho_n^2) \right], \tag{7}$$

$$\mathcal{H}_{\text{eff}} = \frac{1}{8} \left[t_1(2+x_1) + t_2(2+x_2) \right] \tau\rho + \frac{1}{8} \left[t_2(2x_2+1) - t_1(2x_1+1) \right] (\tau_p\rho_p + \tau_n\rho_n), \tag{8}$$

$$\begin{aligned}
\mathcal{H}_{\text{fin}} &= \frac{1}{32} \left[3t_1(2+x_1) - t_2(2+x_2) \right] (\nabla\rho)^2 \\
&\quad - \frac{1}{32} \left[3t_1(2x_1+1) + t_2(2x_2+1) \right] \left[(\nabla\rho_p)^2 + (\nabla\rho_n)^2 \right],
\end{aligned} \tag{9}$$

$$\mathcal{H}_{\text{so}} = \frac{W_0}{2} \left[\mathbf{J}\cdot\nabla\rho + x_w(\mathbf{J_p}\cdot\nabla\rho_p + \mathbf{J_n}\cdot\nabla\rho_n) \right], \tag{10}$$

$$\mathcal{H}_{\text{sg}} = -\frac{1}{16}(t_1 x_1 + t_2 x_2)\mathbf{J}^2 + \frac{1}{16}(t_1 - t_2)\left[\mathbf{J_p}^2 + \mathbf{J_n}^2 \right]. \tag{11}$$

Here, $\rho = \rho_p + \rho_n$, $\tau = \tau_p + \tau_n$, and $\mathbf{J} = \mathbf{J}_p + \mathbf{J}_n$ are the particle number density, kinetic energy density and spin density with p and n denoting the protons and neutrons, respectively. We have used the value of $\hbar^2/2m = 20.734$ MeVfm^2 in our calculations. We would like to emphasize that we have included the contributions from the spin-density term as given by Eq. (11) which is ignored in many Skyrme HF calculations. Although the contributions from the Eq. (11) to the binding energy and charge radii are not very significant, they are very crucial for the calculation of the Landau parameter G_0' [22].

A. Coulomb energy

The contribution to the energy density (Eq. (5)) from the Coulomb interaction can be written as a sum of a direct and an exchange terms,

$$\mathcal{H}_{\text{Coul}}(r) = \mathcal{H}_{\text{Coul}}^{dir}(r) + \mathcal{H}_{\text{Coul}}^{ex}(r). \tag{12}$$

For the direct term it is common to adopt the expression

$$\mathcal{H}_{\text{Coul}}^{dir}(r) = \frac{1}{2}e^2\rho_p(r)\int \frac{\rho_p(r')d^3r'}{|\mathbf{r} - \mathbf{r}'|}, \tag{13}$$

and for the corresponding exchange term to use the Slater approximation [23],

$$\mathcal{H}_{\text{Coul}}^{ex}(r) = -\frac{3}{4}e^2\rho_p(r)\left(\frac{3\rho_p(r)}{\pi}\right)^{1/3}.\tag{14}$$

It is very important to emphasize that the definitions of Eqs. (13) and (14) are not for the bona fide direct and exchange terms, since each of them includes the contributions of the self-interaction, which appear in opposite signs and cancel out in Eq. (12). Note, in particular, that the direct term of Eq. (13) is proportional to Z^2 and not to $Z(Z-1)$, as it should be for a direct term, see a detailed discussion in Ref. [24]. We point out that for the CDE of mirror nuclei the magnitude of the self interaction term is CDE/(2Z), i.e., one has a spurious increase in the calculated CDE of about 6.3% and 2.5% for the A=17 and 41 systems of mirror nuclei, respectively.

We recall that within the mean-field approximation, adjusted to reproduce the experimental values of the charge rms radii, the calculated CDE of analog states (obtained using Eq. (12)) are smaller than the corresponding experimental values by about 7%. It was first shown in Ref. [25] that this discrepancy, also known as the Nolen-Schiffer anomaly [26], can be explained by taking into account the contributions due to long range correlations (LRC) and due to the charge symmetry breaking (CSB) in the NN interaction, see also Ref. [27]. We add that for the mirror nuclei with A=17 and A=41, the LRC and the CSB each accounts for about half of the discrepancy between theory and experiment. Also, the magnitude of the bona fide exchange Coulomb term is about the same as that due to LRC, but with opposite sign. Therefore, neglecting the bona fide Coulomb exchange term does not resolved the discrepancy between theory and experiment, but can account for the contribution of LRC. We add that in Ref. [28], it was shown that by ignoring the Coulomb exchange term in the form of of Eq. (14) in Eq. (12), i.e., by including only the Coulomb direct term in the form of Eq. (13) (as is the case for the SKX interaction), one reproduces the experimental values of the CDE. It should be clear that this is due to the fact that by adopting the form of Eq. (13) for the Coulomb direct term one not only neglects the bona fide Coulomb exchange term, but also adds the spurious contribution of the self-interaction term. The unphysical neglect of the bona fide Coulomb exchange term together with the spurious contribution of the self-interaction term results in a contribution to CDE which is similar in magnitude to that obtained from the LRC + CSB terms. For simplicity, we will adopt in this work the form of Eq. (13) for the Coulomb direct term.

B. Center of mass corrections to the binding energy and charge radii

The HF approach applied to finite nuclei violates the translational invariance, introducing a spurious center of mass (CM) motion. Thus, one must extract the contributions of the center of mass motion to the binding energy B, radii and other observables. An accurate way to restore the translational invariance is to use the projection method. But, it is numerically very expensive. So, it is desirable to develop simple schemes for the CM corrections to various observables. Normally, one makes the CM corrections only to the binding energy and not to the radii. However, the CM corrections to the rms radii for light nuclei may be as large as 2% [24]. In the present work we shall consider the CM corrections to the binding energy as well as charge rms radii used to fit the Skyrme parameters.

To account for the CM correction to the total binding energy, one must subtract from it the so-called CM energy given as,

$$E_{CM} = \frac{1}{2mA}\langle \hat{\mathbf{P}}^2 \rangle \tag{15}$$

where, $\hat{\mathbf{P}} = -i\hbar \sum_{i=1}^{A} \nabla_i$ is the total linear momentum operator. Traditionally, one simplifies the computation of Eq. (15) by taking into account only the one-body parts of it, which can be easily achieved by replacing $\frac{1}{m} \to \frac{1}{m}\left[1 - \frac{1}{A}\right]$, in the kinetic energy term. In this case, the effects of neglecting the two-body part of Eq. (15) are compensated by renormalization of the force parameters. This may induce in the forces an incorrect trend with respect to A which becomes visible in the nuclear matter properties. In fact, it is found in Ref. [29] that an over simplified treatment of E_{CM} obtained by renormalizing the nucleon mass appearing in the kinetic energy term leads to a larger value of the surface energy coefficient than those obtained using the full CM correction. This gives rise to differences in the deformation energy which becomes quite pronounced for the super deformed states. Very recently [17], we also find that a large value of the surface energy coefficient yield a smaller value for the critical density. Thus, an appropriate and still simple scheme to evaluate Eq. (15) is highly desirable. We note, however, that the SLy6, SLy7 and SLy10 interactions [4] have been obtained by evaluating Eq. (15) (i.e., including the one and two-body CM terms of Eq. (15)). In the harmonic oscillator (HO) approximation, E_{CM} of Eq. (15) is given by,

$$E_{CM}^{osc} = \frac{3}{4}\hbar\omega \tag{16}$$

A value of $\hbar\omega = 41A^{-1/3}$ MeV is used in many relativistic mean-field calculations [30, 31]. An improved version for the CM correction can be obtained by modifying the oscillator frequency as $\hbar\omega = 45A^{-1/3} - 25A^{-2/3}$ MeV, which has been used in Ref. [5] to obtain the SKX interaction. Here, we employ a simple but more consistent scheme to evaluate the E_{CM} using the HO approximation. We determine the oscillator frequency $\hbar\omega$ appearing in Eq. (16) using the mean square mass radii $\langle r^2 \rangle$ calculated in the HF approach as,

$$\hbar\omega = \frac{\hbar^2}{mA\langle r^2 \rangle} \sum_i [\mathcal{N}_i + \frac{3}{2}], \tag{17}$$

where, the sum runs over all the occupied single-particle states for the protons and neutrons and $\mathcal{N}_i$ is the oscillator quantum number. We emphasize that this scheme is quite reliable even for the nuclei away from the β-stable line where the values of the rms radii deviate from the $A^{1/3}$ law. We have calculated the total binding energy for the SLy7 interaction using our simple scheme for the CM correction, Eq. (17), and compare them with those given in Ref. [4], obtained by using one-body and two-body parts of the Eq. (15). For example, we find that for the ^{16}O, ^{40}Ca, ^{132}Sn and ^{208}Pb nuclei the total binding energy $B = 128.65$ (128.55), 344.98 (344.90), 1102.38 (1102.77) and 1636.29 (1636.76) MeV, respectively, where the values in parenthesis are taken from Ref. [4]. This clearly indicates that the CM correction to the binding energy can be reliably estimated using Eq. (17). We would also like to remark, however, that the E_{CM} calculated using the oscillator frequency as $\hbar\omega = 45A^{-1/3} - 25A^{-2/3}$ MeV in Eqs. (16) overestimates the value of binding energy in light nuclei (e.g., ^{16}O and ^{40}Ca) by about $1 - 2$ MeV which is quite significant.

The mean-square radius for the point proton distribution corrected for the CM motion is obtained as [24],

$$\langle r_p^2 \rangle = \langle r_p^2 \rangle_{\text{HF}} - \frac{3}{2\nu A}, \tag{18}$$

where, $\nu = m\omega/\hbar$ is the size parameter. Therefore, the corresponding mean-square charge radius to be fitted to the experimental data is obtained as,

$$\langle r_{ch}^2 \rangle = \langle r_p^2 \rangle_{\text{HF}} - \frac{3}{2\nu A} + \langle r^2 \rangle_p + \frac{N}{Z}\langle r^2 \rangle_n + \frac{1}{Z}\left(\frac{\hbar}{mc}\right)\sum_{nlj\tau}(2j+1)\mu_\tau \langle \sigma \cdot l \rangle_{lj}, \tag{19}$$

where, $\langle r^2 \rangle_p$ and $\langle r^2 \rangle_n$ are the mean-squared radii of the proton and neutron charge distributions, respectively. The last term in Eq. (19) is due to the spin-orbit effect [32]. We use, $\langle r^2 \rangle_n = -0.12$ fm^2 and the recent [33] value of $\langle r^2 \rangle_p = 0.801$ fm^2.

C. Determination of the critical density

We use the stability conditions of the Landau parameters for the symmetric nuclear matter and pure neutron matter to calculate the critical density ρ_{cr} for the Skyrme type effective nucleon-nucleon interactions. The stability conditions are given as [34],

$$\mathcal{A}_l > -(2l + 1),\tag{20}$$

where, $\mathcal{A}_l$ stands for the Landau parameters F_l, F_l', G_l and G_l' for a given multipolarity l. Skyrme interactions only contain monopolar and dipolar contributions to the particle-hole interaction so that all Landau parameters are zero for $l > 1$. Thus, there are 12 different Landau parameters, i.e., F_l, F_l', G_l and G_l' ($l = 0, 1$) for the symmetric nuclear matter and $F_l^{(n)}$, $G_l^{(n)}$ ($l = 0, 1$) for the pure neutron matter. Each of these parameters must satisfy the inequality condition given by Eq. (20). Explicit expressions for the Landau parameters in terms of the Skyrme parameters can be found in Refs. [16, 35]. The critical density is nothing but the maximum density beyond which at least one of the Landau Parameter does not satisfy Eq. (20). Following Ref. [16], one can obtain the values of the Landau parameters at any density for a given set of the Skyrme parameters. Thus, for a given set of Skyrme parameters one can easily obtain the value of ρ_{cr}. As mentioned in Sec. I, we include ρ_{cr} in the fit.

D. Breathing mode energy

We also include in our fit the experimental data on the breathing mode energy for several nuclei. We consider the fully self-consistent values for the breathing mode constrained energy defined as,

$$E_0 = \sqrt{\frac{m_1}{m_{-1}}},\tag{21}$$

where m_k are the energy moments

$$m_k = \int_0^\infty \omega^k S(\omega) d\omega,\tag{22}$$

of the strength function

$$S(\omega) = \sum_n |\langle n \mid F \mid 0 \rangle|^2 \delta(\omega - \omega_n),\tag{23}$$

for the monopole operator $F(r) = \sum_{i=1}^{A} f(r_i)$, with $f(r) = r^2$. The moments m_k for $k = -1$ and 1 appearing in Eq. (21) can be obtained using the constrained HF (CHF) and the double commutator sum rule, respectively [36, 37, 38]. The moment m_1 can be expressed in terms of the ground state density ρ as,

$$m_1 = 2\frac{\hbar^2}{m}\langle r^2 \rangle, \tag{24}$$

where,

$$\langle r^2 \rangle = \int r^2 \rho(r) d\mathbf{r}. \tag{25}$$

As described in detail in Ref. [36, 37, 38], m_{-1} can be evaluated via the CHF approach and is given as,

$$m_{-1} = \frac{1}{2}\frac{d}{d\lambda}\langle r_\lambda^2 \rangle \bigg|_{\lambda=0} \tag{26}$$

where, $\langle r_\lambda^2 \rangle = \langle \Phi_\lambda | r^2 | \Phi_\lambda \rangle$, with Φ_λ being the HF solution to the constrained HF Hamiltonian $H - \lambda f$.

III.   SKYRME PARAMETERS AND NUCLEAR MATTER PROPERTIES

In this section we discuss the relationship between the Skyrme parameters and the various quantities describing the nuclear matter. In the next section we use these relations to implement the SAM algorithm. The Skyrme parameters t_i, x_i and α for a fixed value of W_0 can be expressed in terms of the quantities associated with the symmetric nuclear matter as follows [3, 16, 39].

$$
\begin{aligned}
t_0 = {} & \frac{8}{\rho_{nm}} \left[\frac{\left(-B/A + (2m/m^* - 3)\,(\hbar^2/10m)\,k_f^2\right)\left(\frac{1}{27}K_{nm} - (1 - 6m^*/5m)\,(\hbar^2/9m^*)\,k_f^2\right)}{-B/A + \frac{1}{9}K_{nm} - (4m/3m^* - 1)\,(\hbar^2/10m)\,k_f^2} \right. \\
& \left. + \left(1 - \frac{5m}{3m^*}\right)\frac{\hbar^2}{10m}k_f^2 \right],
\end{aligned}
\tag{27}
$$

$$t_1 = \frac{2}{3}\left[T_0 + T_s\right], \tag{28}$$

$$t_2 = t_1 + \frac{8}{3}\left[\left(\frac{1}{4}t_0 + \frac{1}{24}t_3\rho_{nm}^\alpha\right)\frac{2m^*}{\hbar^2}\frac{k_f}{\pi^2} + G_0'\right]\frac{\hbar^2}{m^*\rho_{nm}}, \tag{29}$$

$$t_3 = \frac{16}{\rho_{nm}^{\alpha+1}}\frac{\left(-B/A + (2m/m^* - 3)\,(\hbar^2/10m)\,k_f^2\right)^2}{-B/A + \frac{1}{9}K_{nm} - (4m/3m^* - 1)\,(\hbar^2/10m)\,k_f^2}, \tag{30}$$

10

$$x_0 = \frac{4}{t_0\rho_{nm}} \left[\frac{\hbar^2}{6m}k_f^2 - \frac{1}{24}t_3(x_3 + \frac{1}{2})\rho_{nm}^{\alpha+1} + \frac{1}{24}\left(t_2\left(4 + 5x_2\right) - 3t_1x_1\right)\rho_{nm}k_f^2 - J \right] - \frac{1}{2}, \quad (31)$$

$$x_1 = \frac{1}{t_1} \left[4\frac{\hbar^2\kappa}{m\rho_{nm}} - t_2(2 + x_2) \right] - 2, \quad (32)$$

$$x_2 = \frac{1}{4t_2} \left[8T_0 - 3t_1 - 5t_2 \right], \quad (33)$$

$$x_3 = -\frac{8}{\alpha t_3 \rho_{nm}^{\alpha+1}} \left[\frac{\hbar^2}{6m}k_f^2 - \frac{1}{12}\left((4 + 5x_2)t_2 - 3t_1x_1\right)\rho_{nm}k_f^2 - 3J + L \right] - \frac{1}{2}, \quad (34)$$

$$\alpha = \frac{B/A - \frac{1}{9}K_{nm} + (4m/3m^* - 1)\left(\hbar^2/10m\right)k_f^2}{-B/A + (2m/m^* - 3)\left(\hbar^2/10m\right)k_f^2}, \quad (35)$$

where,

$$T_0 = \frac{1}{8}\left(3t_1 + (5 + 4x_2)t_2\right) = \frac{\hbar^2}{m\rho_{nm}}\left(\frac{m}{m^*} - 1\right), \quad (36)$$

$$T_s = \frac{1}{8}\left[9t_1 - (5 + 4x_2)t_2\right], \quad (37)$$

and

$$k_f = \left(\frac{3\pi^2}{2}\rho_{nm}\right)^{1/3}. \quad (38)$$

In Eqs. (27) - (35), the various quantities characterizing the nuclear matter are the binding energy per nucleon B/A, isoscalar effective mass m^*/m, nuclear matter incompressibility coefficient K_{nm}, symmetry energy coefficient $J = S(\rho = \rho_{nm})$, the coefficient $L = P(\rho = \rho_{nm})$, enhancement factor κ and Landau parameter G'_0. All these quantities are taken at the saturation density ρ_{nm}. It must be pointed out that the expression for the parameter G'_0 used in Eq. (29) includes the contributions from the spin-density term present in the Skyrme energy density functional [22]. So, for consistency, the HF calculations are also performed by including the contributions from the spin density. Once, T_0 is known, T_s can be calculated for a given value of the surface energy E_s as [16],

$$E_s = 8\pi r_0^2 \int_0^{\rho_{nm}} d\rho \left[\frac{\hbar^2}{36m} - \frac{5}{36}T_0\rho + \frac{1}{8}T_s\rho - \frac{m^*}{\hbar^2}V_{so}\rho^2 \right]^{1/2} \left[B(\rho_{nm})/A - B(\rho)/A\right]^{1/2}, \quad (39)$$

11

where, $B(\rho)/A$ is the binding energy per nucleon given by,

$$\frac{B(\rho)}{A} = -\left[\frac{3\hbar^2}{10m^*}k_f^2 + \frac{3}{8}t_0\rho + \frac{1}{16}t_3\rho^{\alpha+1}\right] \tag{40}$$

and,

$$r_0 = \left[\frac{3}{4\pi\rho_{nm}}\right]^{1/3}, \tag{41}$$

$$V_{\text{so}} = \frac{9}{16}W_0{}^2. \tag{42}$$

The manner in which Eqs. (27) - (35) can be used to evaluate the Skyrme parameters t_i, x_i and α is as follows. At first, the parameters t_0 and α can be calculated in terms of B/A, ρ_{nm}, K_{nm} and m^*/m, using Eqs. (27) and (35). Then, the parameter t_3 can be determined using Eq. (30). Next, T_0 and T_s can be calculated using Eqs. (36) and (39), respectively. Once, the combinations T_0 and T_s of the Skyrme parameters are known, one can calculate the remaining parameters in the following sequence, t_1, t_2, x_2, x_1, x_3 and x_0.

IV. SIMULATED ANNEALING BASED ALGORITHM FOR THE MINIMIZATION OF χ^2

The simulated annealing method (SAM) is a generalization of a Monte Carlo technique, based on the Metropolis algorithm [40], initially developed for examining the equation of the state of a many body system. The concept of SAM is based on the manner in which liquids freeze or metals recrystallize in the process of annealing. In an annealing process a metal, initially at high temperature and disordered, slowly cools so that the system at any time is in a thermodynamic equilibrium. As cooling proceeds, the system becomes more ordered and approaches a frozen ground state at zero temperature.

With this brief background, we shall now implement the SAM to search for the global minimum of χ^2 function as given by Eq. (2). One of the crucial key ingredients required to implement the SAM, in the present case, is to specify the lower and the upper limits for each of the Skyrme parameters. So that the global minimum for the χ^2 is searched within these limits. However, from the literature (e.g., see Refs. [8, 39]) we find that the Skyrme parameters vary over a wide range. To make the search process more efficient, we make use of the fact that most of the Skyrme parameters can be expressed in terms of the various quantities related to the nuclear matter properties as described in Sec. III. Most of these

12

nuclear matter quantities are known empirically within $10\% - 20\%$. For convenience, we define a vector $\mathbf{v}$ with 10 components as,

$$\mathbf{v} \equiv (B/A, K_{nm}, \rho_{nm}, m^*/m, E_s, J, L, \kappa, G'_0, W_0). \tag{43}$$

Once the vector $\mathbf{v}$ is known we can calculate the values of all the Skyrme parameters as discussed in Sec. III. We also define the vectors $\mathbf{v}_0$, $\mathbf{v}_1$ and $\mathbf{d}$. The vector $\mathbf{v}_0$ and $\mathbf{v}_1$ contains the lower and the upper limits of each of the components of the vector $\mathbf{v}$. The vector $\mathbf{d}$ represents the maximum displacement allowed in a single step for the components of the vector $\mathbf{v}$. We implement the SAM algorithm using the following basic steps,

(i) We start with a guess value for the vector $\mathbf{v}$ and calculate χ^2 (say, χ^2_{old}) using Eq. (2) for a given set of the experimental data and the corresponding HF results together with the theoretical errors.

(ii) We generate randomly a new set of Skyrme parameters using the following steps. First, we use a uniform random number to select a component v_r of the vector $\mathbf{v}$. Second, the randomly selected component v_r is then assigned a new value,

$$v_r \rightarrow v_r + \eta d_r, \tag{44}$$

where η is a uniform random number which lies within the range of -1 to $+1$. The second step is repeated until the new value of v_r is found within its allowed limits defined by $\mathbf{v}_0$ and $\mathbf{v}_1$. We use this modified $\mathbf{v}$ to generate a new set of Skyrme parameters. It may be noted that a change in the value of a component of the vector $\mathbf{v}$ may lead to changes in the values of several Skyrme parameters. For example, a change in the value of K_{nm} will alter the values of the Skyrme parameters t_0, t_3 and α.

(iii) The newly generated set of the Skyrme parameters is accepted by using the Metropolis algorithm as follows. We calculate the quantity,

$$\mathcal{P}(\chi^2) = e^{(\chi^2_{\text{old}} - \chi^2_{\text{new}})/T}, \tag{45}$$

where χ^2_{new} is obtained by using the newly generated set of the Skyrme parameters and T is a control parameter (an effective temperature). The new set of Skyrme parameters is accepted only if,

$$\mathcal{P}(\chi^2) > \beta, \tag{46}$$

13

where β is a uniform random number which lies between 0 and 1. If the new Skyrme parameters are accepted (i.e. Eq. (46) is satisfied), it is called a "successful reconfiguration".

To search for the global minimum of χ^2 we begin with some reasonable value of an effective temperature $T = T_i$. For a given T_i, we repeat steps (ii) and (iii) for, say, $100N_p$ reconfigurations, or for $10N_p$ successful reconfigurations, whichever comes first. Then, we reduce the temperature by following a suitable annealing schedule. One encounters various annealing schedule available in the literature such as linear, exponential, Boltzmann and Cauchy annealing schedules [13]. Among these, the Boltzmann annealing schedule is the slowest one and the exponential annealing schedule is the fastest one. In the present work we have employed the Cauchy annealing schedule given by,

$$T(k) = T_i/ck \tag{47}$$

where, c is a constant, which is taken to be unity in the present work, and $k = 1, 2, 3, ...$ is the time index. We keep on reducing the value of T using Eq. (47) in the subsequent steps until the effort to reduce the value of χ^2 further becomes sufficiently discouraging.

In Table I we list the values of all the components of the vectors $\mathbf{v}$, $\mathbf{v}_0$, $\mathbf{v}_1$ and $\mathbf{d}$ used in the numerical computation. We have varied the components of the vector $\mathbf{v}$ over a wide range. The values of the maximum displacement as defined by the components of $\mathbf{d}$ are so chosen that the corresponding component of the vector $\mathbf{v}$ can be varied over the entire range given by the vectors $\mathbf{v_0}$ and $\mathbf{v_1}$, within the adopted number of reconfigurations. We have carried out several sample runs and found that $T_i = 1.25$ along with the Cauchy annealing schedule yields reasonable values of the Skyrme parameters. We must mention here that the range for the quantities L, κ and G'_0 as given in Table I are so chosen that they vary within acceptable limits [17].

V.   EXPERIMENTAL DATA AND SOME CONSTRAINTS

In this section we discuss our selection of the experimental data and the corresponding theoretical errors adopted in the χ^2 fit, Eq. (2), to the HF results. In Table II we summarize our choice of the experimental data. It must be noted that in addition to the typically used data on the binding energy, charge radii and spin-orbit splitting, we also include in our fit the

experimental data for the radii of valence neutron orbits and the breathing mode energies of several nuclei. All of these experimental data are taken from Refs. [41, 42, 43, 44, 45, 46, 47]. For the binding energy we use in our fit the error of 1.0 MeV except for the ^{100}Sn nuclei. The binding energy for the ^{100}Sn nucleus is determined from systematics and are expected to have large errors. Thus, we assign them a theoretical error of 2.0 MeV. For the charge rms radii we use the theoretical error of 0.02 fm except for the case of ^{56}Ni nucleus. The charge rms radii for the ^{56}Ni nucleus is obtained from systematics and we use the theoretical error of 0.04 fm. We consider in our fit the experimental data for the spin-orbit splittings for the $2p$ neutrons and protons in the ^{56}Ni nucleus and the rms radii for the $1d_{5/2}$ and $1f_{7/2}$ neutron orbits in ^{17}O and ^{41}Ca nuclei, respectively. We use [46],

$$\epsilon(2p_{1/2}) - \epsilon(2p_{3/2}) = \begin{cases} 1.88\,\text{MeV} & \text{Neutrons} \\ 1.83\,\text{MeV} & \text{Protons} \end{cases} \tag{48}$$

where, ϵ is the "bare" single-particle energy obtained by unfolding the experimental data for the energy levels in ^{57}Ni and ^{57}Cu nuclei by appropriately accounting for the coupling to excitations of the core. Of course, it is more appropriate to use the splitting of high l orbits in a heavy nucleus (e.g., ^{208}Pb nucleus) to determine the strength of the spin-orbit interaction. But, to the best of our knowledge, unlike for the ^{56}Ni nucleus the bare single-particle energies for the heavier nuclei are not available. For the rms radii of the valence neutron orbits in ^{17}O and ^{41}Ca nuclei we use $r_v(\nu 1d_{5/2}) = 3.36$ fm and $r_v(\nu 1f_{7/2}) = 3.99$ fm, [44, 45] respectively. The theoretical error taken for the spin-orbit splitting data is 0.2 MeV and for the rms radii for the valence neutron orbits we use the experimental error of 0.06 fm. We must point out that the choice of the theoretical error on the rms radii for the valence neutron orbits is due to the large uncertainties associated with their extraction from the experimental measurements. To be consistent with the way these valence neutron radii are determined, we do not include the center of mass correction to these data. The experimental data for the breathing mode constrained energies E_0 included in our fit are 17.81, 15.90, 15.25 and 14.18 MeV for the ^{90}Zr, ^{116}Sn, ^{144}Sm and ^{208}Pb nuclei [47], respectively, with the theoretical error taken to be 0.5 MeV for the ^{90}Zr nucleus and 0.3 MeV for the other nuclei. We also include the critical density ρ_{cr} in the fit assuming a value of $2.5\rho_0$ with an error of $0.5\rho_0$. Further the values of the Skyrme parameters are constrained by requiring that (i) $P \geqslant 0$ for $\rho \leqslant 3\rho_0$, (ii) $\kappa = 0.1 - 0.5$ and (iii) $G_0' \geqslant 0$ at $\rho = \rho_0$.

VI. RESULTS AND DISCUSSIONS

In the preceding sections we have described in detail the implementation of the SAM based algorithm to fit the values of the Skyrme parameters to a given set of the experimental data considered in this work. We have carried out two different fits. These fits are carried out by using the same set of experimental data along with some constraints as discussed in Sec. V. We name these fits as,

1. KDE0; only the direct Coulomb term in the form of Eq. (13) is included.

2. KDE; the direct as well as the exchange Coulomb terms are included (Eqs. (12)-(14)).

The CM corrections to the total binding energy, Eqs. (16) and (17), and the charge rms radii, Eqs. (18) and (19), are carried out using the schemes described in Sec. II B.

We shall first consider some technical aspects required to implement the SAM. As it is evident from Sec. IV, there are two crucial ingredients, namely, (i) initial value for the control parameter $T = T_i$ and (ii) annealing schedule which determines the subsequent value for T. These ingredients essentially controls the computer time and the quality of the final fit. If one starts with a smaller value for T_i and/or uses a faster annealing schedule, one may not be able to hit the global minimum of the objective function and rather get trapped in one of the local minima. In the present work we have employed the Cauchy annealing schedule. We have carried out several trial calculations and find that $T_i = 1.25$, along with the Cauchy's annealing schedule as given by Eq. (47), yields reasonable values for the best fit parameters. To validate the present approach we carried out the following checks. Starting with the final values of the Skyrme parameters obtained using the SAM, we attempted to minimize further the value of χ^2 using the Levenberg-Marquardt (LM) method [10] as conventionally used. But, we found no further decrease in the value of the χ^2. As an illustration, we plot in Fig. 1 the average value $\langle \chi^2 \rangle_T$ as an inverse function of the control parameter T for the KDE0 case. The curves labeled v and v_1 represent the results obtained from two different choices of the starting values for the Skyrme parameters. The initial value of the Skyrme parameters for the curve labeled v (solid line) and v_1 (dashed line) are obtained using the set of values given in the second and fourth columns of Table I, respectively. The value of $\langle \chi^2 \rangle_T$ is obtained by averaging over all the successful reconfigurations for a given T. We see from Fig. 1 that the value of $\langle \chi^2 \rangle_T$ show a remarkable decrease at initial stages and then

oscillates before saturating to a minimum value for $T \leqslant 0.05$. The value of χ^2 at lower T is more or less independent of the starting values for the Skyrme parameters. In Fig 2 we have displayed the variation of $\Delta\chi_T^2 = \langle(\chi^2 - \langle\chi^2\rangle)^2\rangle_T$ as an inverse function of T. We see that the fluctuations in the value of χ^2 is large for larger values of T. As T decreases, fluctuations in the value of χ^2 also decrease rapidly. This means that initial value for T should not be too small, because, at smaller T it is less likely to jump from a configuration with lower value of χ^2 to one having higher value. As a result, one may get trapped in a local minima. In Table III we give the values of the parameters for the KDE0 interaction at the minimum value of the χ^2 obtained from different choices for the starting values for the Skyrme parameters. It is interesting to note that not only the final value of the χ^2 is less sensitive to the choice of the initial parameters, but, also the resulting Skyrme parameters are also quite close. In what follows, we shall present the results for the KDE0 and KDE interactions. The starting (or guess) values for he Skyrme parameters used to generate these interactions are obtained from the nuclear matter quantities given in the second column of the Table I.

In Table IV we give the values for the various quantities characterizing the nuclear matter obtained at the minimum value of the χ^2. We also note that the values of all the nuclear matter properties for the KDE0 and KDE Skyrme interaction are closer to those obtained for the SLy7 interaction. However, it is worth mentioning that the values of the K_{nm} and m^*/m for both the interactions generated here emerge from the fit, unlike the SLy type interactions where the values for these quantities were kept fixed. In our fits, the values of the K_{nm} and m^*/m are mainly constrained by the inclusion of the experimental data on breathing mode energy and the value of critical density $\rho_{cr} = 2.5\rho_0 \pm 0.5\rho_0$ [16, 17]. In the last row of this table we give the values of χ^2 at the minimum. For the sake of completeness, we list in Table V the values of the Skyrme parameters obtained in the fits. One can easily calculate the values of these Skyrme parameters using the various nuclear matter quantities given in Table IV as described in Sec. III. In Table V we also give in parenthesis the values of the standard deviations for the Skyrme parameters. Since, within the SAM algorithm one can not calculate these standard deviations in a straight forward manner, we resort to some alternative approach. We have determined the values of the standard deviations on the parameters for the KDE0 and KDE interactions using the LM method. The LM method requires two inputs, namely, set of the experimental data and the starting values of the interaction parameters. The set of experimental data is taken to be exactly the same

as the one used to generate the KDE0 and KDE interactions. The starting values of the interactions parameters used are the ones obtained using SAM for the KDE0 and KDE interactions.

In Table VI we present our results for the deviation $\Delta B = B^{exp} - B^{th}$ for the values of the binding energy obtained from the newly generated KDE0 and KDE interactions. Similar deviations Δr_{ch} for the charge rms radii are presented in Table VII. For comparison, in the last columns of these Tables we give the values of ΔB and Δr_{ch} for the SLy7 interaction, taken from Ref. [4]. One can easily verify from Table VI that the magnitude of the deviations for the binding energy for most of the cases is much less than 0.5% in case of KDE0 interaction. The KDE interaction yields larger error in the values of the binding energy ($\sim 0.6 - 1.0\%$) for the ^{16}O, ^{48}Ni and ^{100}Sn nuclei. We would also like to remark here that in determining the SKX interaction, the binding energy for the ^{56}Ni nucleus was not considered in the fit and that for the ^{100}Sn nucleus was included in the fit with the theoretical error of 1.0 MeV. We find that if one attempt to do so, the binding energy for the ^{56}Ni becomes off by more than 3 MeV. We see from Table VII that, except for the ^{16}O and ^{48}ca nuclei, the deviations in the values of the charge rms radii for the KDE0 interaction is less than 0.5%. In addition to the binding energy and the charge rms radii of the nuclei used in our fits, we have also considered a few more experimental data as discussed in Sec. V. In Tables VIII and IX we present our results for these additional quantities. The values of ρ_{cr} is greater than $2\rho_0$. The values for the radii of valence neutron orbits and the spin-orbit splittings considered in our fits are quite reasonable for all the interactions considered here. It can be seen from Table IX that our fit to the breathing mode constrained energies are overall in reasonable agreement with the corresponding experimental data.

We now consider our results for the binding energy difference between the ^{48}Ca and ^{48}Ni mirror nuclei. One may verify from Table VI that the binding energy difference $B(^{48}$Ca$) - B(^{48}$Ni$) = 67.23$ and 64.02 MeV for the KDE0 and KDE interactions, respectively, compared to the experimental value of 68.85 MeV. We would also like to add that the said difference for the SKX interaction is 66.3 MeV which is about 1.0 MeV lower than our most realistic KDE0 interaction. On the other hand, most of the Skyrme interactions which include the contribution from the exchange Coulomb term yield $B(^{48}$Ca$) - B(^{48}$Ni$) \approx 63$ MeV, which is about 6 MeV lower than the corresponding experimental value.

We present in Table X our results for the neutron skin, $r_n - r_p$, the difference between the rms radii for the point neutrons and protons density distributions, for the KDE0 and KDE interactions. We compare in Tables XI and XII the values of the single-particle energies with the available experimental data for the ^{40}Ca and ^{208}Pb nuclei [48, 49], respectively. We find that the single-particle energies, for the occupied states near the fermi-energy compare reasonably well with the experimental ones. We would like to remark here that the HF approach alone is not expected to reproduce the experimental single-particle energies and there fore we have not included them in our fit.

Finally, we consider the behavior of the symmetry energy coefficient $S(\rho)$ for densities relevant to the study of neutron stars. It is well known [50, 51] that the values of $S(\rho)$ and the resulting EOS for pure neutron matter at higher densities ($\rho > 2\rho_0$) are crucial in understanding the various properties of neutron star. For example, the proton fraction at any density depends strongly on the value of $S(\rho)$ at that density, which in turn affects the chemical compositions as well as the cooling mechanism of the neutron star [52]. Yet, no consensus is reached for the density dependence of $S(\rho)$. We display in Fig. 3, our results for the variation of the symmetry energy S as a function of the nuclear matter density ρ. We see for the KDE0 and KDE interactions that the value of S increases with density for $\rho < 3\rho_0$. All of these interactions are quite suitable for modeling the neutron star with masses close to the canonical one [8], because, they yield $S > 0$ for $\rho < 4\rho_0$. In Fig. 4 we plot the EOS for the pure neutron matter resulting from the KDE0 and KDE interactions and compare them with the ones obtained for SLy7 interaction and the realistic UV14+UVII model [53]. It is striking to note that our results for the KDE0 and KDE interactions are in harmony with the EOS for the UV14+UVII model, though, unlike the SLy7 interaction we did not include in our fit the neutron matter EOS of the realistic UV14+UVII interaction. This seems to be due to the constrain imposed on the quantity P, which is related to the slope of the symmetry energy coefficient (see Eq. (1)).

VII.   CONCLUSIONS

We have implemented the simulated annealing method to fit the values of the parameters of the Skyrme interaction of Eq. (3) by searching for the global minimum in the hyper surface of the χ^2 function, Eq. (2). To demonstrate the applicability of this method we have fitted

the values of the Skyrme parameters to an extensive set of experimental data together with a few additional constraints. Our experimental data set consists of the binding energies for 14 nuclei ranging from the normal to exotic (proton or neutron rich) ones, charge rms radii for 7 nuclei, spin-orbit splittings for the $2p$ proton and neutron orbits of the ^{56}Ni nucleus and rms radii for $1d_{5/2}$ and $1f_{7/2}$ valence neutron orbits in the ^{17}O and ^{41}Ca nuclei, respectively. We also include in the fit the critical density ρ_{cr} determined from the stability conditions for the Landau parameters. The additional constraints imposed on the Skyrme parameters are (i) the quantity $P = 3\rho \frac{dS}{d\rho}$, directly related to the slope of the symmetry energy S, must be positive for densities up to $3\rho_0$; a condition imposed by the neutron star models [8], (ii) the enhancement factor κ, associated with the TRK sum rule for the isovector giant dipole resonance, should lie in the range of $0.1 - 0.5$ and (iii) the Landau parameter G'_0, crucial for the spin properties of finite nuclei and nuclear matter, should be positive at $\rho = \rho_0$.

Using these experimental data along with the additional constrains, we have carried out two different fits named as KDE0 and KDE, as described in Sec. VI. The corrections to the binding energy and charge rms radii due to the center of mass motion were performed using simple but consistent schemes. The nuclear matter properties for both interactions proposed in the present work are obtained directly from the fit. The selection of the experimental data in conjugation with some constraints ensures that these interactions can be used to study the bulk ground state properties of nuclei ranging from the stable to the ones near the proton and neutron drip lines, as well as the properties of neutron stars. The interactions obtained in the present work encompasses the merits of the SKX and SLy type of Skyrme interactions.

Before closing, we would like to mention that the method as well as the fitting strategy presented in this work can be improved in several ways. The SAM is a very adaptive approach and therefore it offers a significant scope for further improvement. For example, in the present work we jump from one configuration to another by randomly selecting a component of the vector $\mathbf{v}$ as defined by Eq. (43). This selection was done using a uniform random number. However, one can think of performing random selection of a component of $\mathbf{v}$ by assigning a more plausible weight factors to these components. One can also try out different annealing schedules to determine the rate of cooling. In the present work we employed the Cauchy annealing schedule which yields a faster cooling rate than that of the Boltzmann schedule, but, a slower rate than the exponential annealing schedule. The effects

on the binding energy and radii due to the correlations beyond mean-field [54, 55, 56] can be included in the fit. These effects are in particular important for the light nuclei. One may also include in the spin-orbit splitting the contributions due to the electromagnetic spin-orbit interaction [46] and modify the spin-orbit interaction by using the form proposed by Sagawa in Ref. [57]. Last but not least, one may also include the experimental data on the giant dipole and quadrupole resonances while fitting the Skyrme parameters in addition to the breathing mode energy, as was done in the present work.

Acknowledgments

[1] D. Vautherin and D. M. Brink, Phys. Rev. C **5**, 626 (1972).

[2] P. G. Reinhard and H. Flocard, Nucl. Phys. **A584**, 467 (1995).

[3] E. Chabanat, P. Bonche, P. Haensel, J. Meyer, and R. Schaeffer, Nucl. Phys. **A627**, 710 (1997).

[4] E. Chabanat, P. Bonche, P. Haensel, J. Meyer, and R. Schaeffer, Nucl. Phys. **A635**, 231 (1998).

[5] B. A. Brown, Phy. Rev. C **58**, 220 (1998).

[6] P. G. Reinhard, D. J. Dean, W. Nazarewicz, J. Dobaczewski, J. A. Maruhn, and M. R. Strayer, Phys. Rev. C **60**, 014316 (1999).

[7] M. Bender, P. H. Heenen, and P.-G. Reinhard, Rev. Mod. Phys. **75**, 121 (2003).

[8] J. R. Stone, J. C. Miller, R. Koncewicz, P. D. Stevenson, and M. R. Strayer, Phys. Rev. C **68**, 034324 (2003).

[9] S. Krikpatrik, C. D. Gelatt, Jr., and M. P. Vecchi, Science **220**, 671 (1983).

[10] W. H. Press, S. A. Teukolsky, W. T. Vetterling, and B. P. Flannery, *Numerical Recipes in Fortran* (Cambridge University Press, 1992).

[11] S. Krikpatrik, J. Stat. Phys. **34**, 975 (1984).

[12] L. Ingber, Mathl. Comput. Modelling **12**, 967 (1989).

[13] B. Cohen, Master's thesis, Tel-Aviv University (1994).

[14] T. Brvenich, D. G. Madland, J. A. Maruhn, and P.-G. Reinhard, Phys. Rev. C **65**, 044308 (2002).

[15] T. Brvenich, D. G. Madland, and P.-G. Reinhard, nucl-th/0407036.

[16] J. Margueron, J. Navarro, and N. V. Giai, Phys. Rev. C **66**, 014303 (2002).

[17] B. K. Agrawal, S. Shlomo, and V. K. Au, Phys. Rev. C **70**, 057302 (2004).

[18] B. L. Berman and S. C. Fultz, Rev. Mod. Phys. **47**, 713 (1975).

[19] H. Krivine, J. Treiner, and O. Bohigas, Nucl. Phys. **A336**, 155 (1980).

[20] K.-F. Liu, H. Luo, Z. Ma, Q. Shen, and S. A. Mozkowski, Nucl. Phys. **A534**, 25 (1991).

[21] K.-F. Liu, H. Luo, Z. Ma, and Q. Shen, Nucl. Phys. **A534**, 1 (1991).

[22] M. Bender, J. Dobaczewski, J. Engel, and W. Nazarewicz, Phys. Rev. C **65**, 054322 (2002).

[23] M. J. Giannoni and P. Quentin, Phys. Rev. C **21**, 2076 (1980).

[24] S. Shlomo, Rep. Prog. Phys. **41**, 957 (1978).

[25] S. Shlomo and W. G. Love, Phys. Scr. **26**, 280 (1982).

[26] J. A. Nolen and J. P. Schiffer, Annu. Rev. Nucl. Sci. **19**, 471 (1969).

[27] B. K. Agrawal, T. Sil, S. K. Samaddar, J. N. De, and S. Shlomo, Phys. Rev. C **64**, 024305 (2001).

[28] B. A. Brown, W. A. Richter, and R. Lindsay, Phys. Lett. B **483**, 49 (2000).

[29] M. Bender, K. Rutz, P. G. Reinhard, and J. A. Maruhn, Eur. Phys. J. A **7**, 467 (2000).

[30] G. A. Lalazissis, J. Konig, and P. Ring, Phys. Rev. C **55**, 540 (1997).

[31] P. Ring, Y. K. Gambhir, and G. A. Lalazissis, Comp. Phys. Comm. **105**, 77 (1997).

[32] W. Bertozzi, J. Friar, J. Heisenberg, and J. W. Negele, Phys. Lett. B **4**, 408 (1972).

[33] I. Sick, Phys. Lett. **B576**, 62 (2003).

[34] A. B. Migdal, *Theory of finite Fermi system and application to atomic nuclei* (Interscience, London, 1967).

[35] S. Krewald, V. Klemt, J. Speth, and A. Faessler, Nucl. Phys. **A281**, 166 (1977).

[36] O. Bohigas, A. M. Lane, and J. Martorell, Phys. Rep. **51**, 267 (1979).

[37] G. Colo and N. V. Giai, Nucl. Phys. **A731**, 15c (2004).

[38] B. K. Agrawal, S. Shlomo, and V. K. Au, Phys. Rev. C **70**, 014308 (2004).

[39] J. M. G. Gomez, C. Prieto, and J. Navarro, Nucl. Phys. **A549**, 125 (1992).

[40] N. Metropolis, A. W. Rosenbluth, M. N. Rosenbluth, A. H. Teller, and E. Teller, J. Chem. Phys. **21**, 1087 (1953).

[41] G. Audi, A. H. Wapstra, and C. Thibault, Nucl. Phys. **A729**, 337 (2003).

[42] E. W. Otten, *in Treatise on Heavy-Ion Science*, vol. 8 (ed. D. A. Bromley, Plenum, New York, 1989).

[43] H. D. Vries, C. W. D. Jager, and C. D. Vries, At. Data Nucl. Data Tables **36**, 495 (1987).

[44] N. Kalantar-Nayestanaki et al., Phys. Rev. Lett. **60**, 1707 (1988).

[45] S. Platchkov et al., Phys. Rev. Lett. **61**, 1465 (1988).

[46] L. Trache, A. Kolomiets, S. Shlomo, K. Heyde, C. A. Gagliardi, R. E. Tribble, X. G. Zhou, V. E. Iacob, and A. M. Oros, Phys. Rev. C **54**, 2361 (1996).

[47] D. H. Youngblood, H. L. Clark, and Y. W. Lui, Phys. Rev. Lett. **82**, 691 (1999).

[48] A. Bohr and B. Mottelson, *Nuclear Structure*, vol. Vol. I (Benjamin, New York, 1969).

[49] A. N. James, P. T. Andrews, P. Kirkby, and B. G. Lowe, Nucl. Phys. **A138**, 145 (1969).

[50] M. Kutschera, Phys. Lett. **B340**, 1 (1994).

[51] M. Kutschera and J. Niemiec, Phys. Rev. C **62**, 025802 (2000).

[52] J. M. Lattimer, C. J. Pethick, M.Prakash, and P. Haensel, Phys. Rev. Lett. **66**, 2701 (1991).

[53] R. Wiringa, V. Fiks, and A. Fabrocini, Phys. Rev. C **38**, 1010 (1988).

[54] H. Esbensen and G. F. Bertsch, Phys. Rev. C **28**, 355 (1983).

[55] S. Shlomo, Phys. Lett. B **209**, 23 (1988).

[56] M. Bender, G. F. Bertsch, and P.-H. Heenen, Phys. Rev. C **69**, 034340 (2004).

[57] H. Sagawa and S. Yoshida, Nucl. Phys. **A688**, 755 (2001).

Figure captions

FIG. 1:   Variation of the average value of chi-square, $\langle \chi^2 \rangle_T$, as a function of the inverse of the control parameter T for the KDE0 interaction for the two different choices of the starting parameters (see text for detail).

FIG. 2:   Variation of the fluctuations $\Delta \chi_T^2$ in the value of χ^2 as a function of $1/T$ for the KDE0 interaction for the two different choices of the starting parameters (see text for detail).

FIG. 3:   Variation of the symmetry energy coefficient $S(\rho)$ as a function of the nuclear matter density ρ.

FIG. 4:   Energy per particle for pure neutron matter $E^{(n)}/A$ as a function of density. Results for the two newly generated Skyrme interactions KDE0 and KDE are compared with those obtained for the SLy7 Skyrme force and the realistic UV14+UVII model of Wiringa et al. [53].

TABLE I: Values of the components of the vectors $\mathbf{v}$, $\mathbf{v}_0$, $\mathbf{v}_1$ and $\mathbf{d}$ used for implementing the SAM based algorithm for searching the global minimum of χ^2 . The vector $\mathbf{v}$ initializes the value of χ^2, whereas, $\mathbf{v}_0$ and $\mathbf{v}_1$ limits the search space for the Skyrme parameters. The components of the vector $\mathbf{d}$ correspond to the maximum displacements allowed for the reconfiguration.

	$\mathbf{v}$	$\mathbf{v}_0$	$\mathbf{v}_1$	$\mathbf{d}$
$B/A(\text{MeV})$	16.0	17.0	15.0	0.40
$K_{nm}(\text{MeV})$	230.0	200.0	300.0	20.0
$\rho_{nm}(\text{fm}^{-3})$	0.160	0.150	0.170	0.005
m^*/m	0.70	0.60	0.90	0.04
$E_s(\text{MeV})$	18.0	17.0	19.0	0.3
$J(\text{MeV})$	32.0	25.0	40.0	4.0
$L(\text{MeV})$	47.0	20.0	80.0	10.0
κ	0.25	0.1	0.5	0.1
G_0'	0.08	0.00	0.40	0.10
W_0 (MeV.fm^5)	120.0	100.0	150.0	5.0

TABLE II: Selected experimental data for the binding energy B, charge rms radius r_{ch}, rms radii of valence neutron orbits r_v, spin-orbit splitting S-O, breathing mode constrained energy E_0 and critical density ρ_{cr} used in the fit to determine the parameters of the Skyrme interaction.

Properties	Nuclei	Ref.
B	^{16,24}O, ^{34}Si, ^{40,48}Ca, ^{48,56,68,78}Ni, ^{88}Sr, ^{90}Zr, ^{100,132}Sn, ^{208}Pb	[41]
r_{ch}	^{16}O, ^{40,48}Ca, ^{56}Ni, ^{88}Sr, ^{90}Zr, ^{208}Pb	[42, 43]
$r_v(\nu 1d_{5/2})$	^{17}O	[44]
$r_v(\nu 1f_{7/2})$	^{41}Ca	[45]
S-O	$2p$ orbits in ^{56}Ni	[46]
E_o	^{90}Zr, ^{116}Sn, ^{144}Sm, ^{208}Pb	[47]
ρ_{cr}	nuclear matter	see text

TABLE III: Comparison of the parameters for the KDE0 interaction at the minimum value of χ^2 obtained from different choices for the starting values of the Skyrme parameters.

Parameter	KDE0($\mathbf{v}$)	KDE0($\mathbf{v}_1$)
t_0(MeV·fm^3)	-2526.51	-2553.08
t_1(MeV·fm^5)	430.94	411.70
t_2(MeV·fm^5)	-398.38	-419.87
t_3 (MeV·fm$^{3(1+\alpha)}$)	14235.5	14603.6
x_0	0.7583	0.6483
x_1	-0.3087	-0.3472
x_2	-0.9495	-0.9268
x_3	1.1445	0.9475
W_0(MeV·fm^5)	128.96	124.41
α	0.1676	0.1673

TABLE IV: Nuclear matter properties for the KDE0 and KDE interactions at the $\chi^2 = \chi^2_{min}$.

Parameter	KDE0	KDE	SLy7
B/A (MeV)	16.11	15.99	15.92
K_{nm}(MeV)	228.82	223.89	229.7
ρ_{nm}	0.161	0.164	0.158
m^*/m	0.72	0.76	0.69
E_s (MeV)	17.91	17.98	17.89
J (MeV)	33.00	31.97	31.99
L (MeV)	45.22	41.43	47.21
κ	0.30	0.16	0.25
G'_0	0.05	0.03	0.04
χ^2_{min}	1.3	2.2	

TABLE V: The values of the Skyrme parameters for KDE0 and KDE interactions obtained by minimizing the χ^2. For the sake of comparison we have also listed the values of the parameters for the SLy7 interaction. The values in Parenthesis are the standard deviation for the corresponding Skyrme parameters.

Parameter	KDE0	KDE	SLy7
$t_0(\text{MeV}\cdot\text{fm}^3)$	-2526.51 (140.63)	-2532.88 (115.32)	-2482.41
t_1 (MeV·fm^5)	430.94 (16.67)	403.73 (27.63)	457.97
t_2 (MeV·fm^5)	-398.38 (27.31)	-394.56 (14.26)	-419.85
$t_3(\text{MeV}\cdot\text{fm}^{3(1+\alpha)})$	14235.5 (680.73)	14575.0 (641.99)	13677.0
x_0	0.7583 (0.0655)	0.7707 (0.0579)	0.8460
x_1	-0.3087 (0.0165)	-0.5229 (0.0298)	-0.5110
x_2	-0.9495 (0.0179)	-0.8956 (0.0270)	-1.0000
x_3	1.1445 (0.0862)	1.1716 (0.0767)	1.3910
W_0 (MeV·fm^5)	128.96 (3.33)	128.06 (4.39)	126.00
α	0.1676 (0.0163)	0.1690 (0.0144)	0.1667

TABLE VI: Results for the total binding energy B (in MeV) for several nuclei. The experimental data B^{exp} used to fit the Skyrme parameters were taken from [41]. The theoretical error σ was taken to be 2.0 MeV for the ^{100}Sn nucleus and 1.0 MeV for the other nuclei. In 3rd and 4th columns we give the values for $\Delta B = B^{exp} - B^{th}$ obtained from our new fits. The last column contains the values for ΔB for the SLy7 Skyrme interaction taken from Ref. [4].

| Nuclei | B^{exp} | $\Delta B = B^{exp} - B^{th}$ | | |
		KDE0	KDE	SLy7
^{16}O	127.620	0.394	1.011	−0.93
^{24}O	168.384	−0.581	0.370	
^{34}Si	283.427	−0.656	0.060	
^{40}Ca	342.050	0.005	0.252	−2.85
^{48}Ca	415.990	0.188	1.165	0.11
^{48}Ni	347.136	−1.437	−3.670	
^{56}Ni	483.991	1.091	1.016	1.71
^{68}Ni	590.408	0.169	0.539	1.06
^{78}Ni	641.940	−0.252	0.763	
^{88}Sr	768.468	0.826	1.132	
^{90}Zr	783.892	−0.127	−0.200	
^{100}Sn	824.800	−3.664	−4.928	−4.83
^{132}Sn	1102.850	−0.422	−0.314	0.08
^{208}Pb	1636.430	0.945	−0.338	−0.33

TABLE VII: Results for the charge root mean square (rms) radii r_{ch} (in fm). The experimental data used in the fit to determine the values of the Skyrme parameters are taken from Refs. [42, 43]. The theoretical error σ taken to be 0.04 fm for the ^{56}Ni nucleus and 0.02 fm for the other nuclei. In 3rd and 4th columns we give the values for $\Delta r_{ch} = r_{ch}^{exp} - r_{ch}^{th}$ obtained from our new fits. The last column contains the values for Δr_{ch} for the SLy7 Skyrme interaction taken from Ref. [4].

| Nuclei | r_{ch}^{exp} | $\Delta r_{ch} = r_{ch}^{exp} - r_{ch}^{th}$ | | |
		KDE0	KDE	SLy7
^{16}O	2.730	-0.041	-0.039	-0.017
^{40}Ca	3.490	0.000	0.011	0.020
^{48}Ca	3.480	-0.021	-0.008	-0.015
^{56}Ni	3.750	-0.018	0.000	-0.008
^{88}Sr	4.219	-0.002	0.019	
^{90}Zr	4.258	-0.008	0.013	
^{208}Pb	5.500	0.011	0.041	0.002

TABLE VIII: Critical density ρ_{cr}, rms radii of the valence neutron orbits r_v and spin-orbit splitting (S-O). The experimental values (and the theoretical error σ) used in the fit to determine the Skyrme parameters are taken as follows: for the ρ_{cr} we assume a value of $2.5\rho_0$ ($\sigma = 0.5\rho_0$), the values of r_v were taken from Ref. [44, 45] ($\sigma = 0.06$ fm) and the spin-orbit in ^{56}Ni were taken from Ref. [46] ($\sigma = 0.2$ MeV). In columns $3 - 6$ we give the results obtained from our new fits.

	Expt.	KDE0	KDE
ρ_{cr}/ρ_0	2.5	2.5	2.1
$r_v(\nu 1d_{5/2})$(fm)	3.36	3.42	3.41
$r_v(\nu 1f_{7/2})$(fm)	3.99	4.05	4.03
$\epsilon_n(2p_{1/2}) - \epsilon_n(2p_{3/2})$ (MeV)	1.88	1.84	1.81
$\epsilon_p(2p_{1/2}) - \epsilon_p(2p_{3/2})$ (MeV)	1.83	1.64	1.63

TABLE IX: Comparison of the breathing mode constrained energies (in MeV) obtained for the KDE0 and KDE interactions with the experimental data.

Nucleus	Expt.	KDE0	KDE
^{90}Zr	17.81	17.98	17.91
^{116}Sn	15.90	16.42	16.36
^{144}Sm	15.25	15.53	15.47
^{208}Pb	14.18	13.64	13.60

TABLE X: Results for the neutron skin, $r_n - r_p$ (in fm), for all the nuclei considered to obtain the KDE0 and KDE interactions.

Nuclei	$r_n - r_p$	
	KDE0	KDE
^{16}O	-0.031	-0.025
^{24}O	0.510	0.510
^{34}SI	0.189	0.192
^{40}CA	-0.051	-0.046
^{48}CA	0.158	0.159
^{48}NI	-0.282	-0.274
^{56}NI	-0.056	-0.052
^{68}NI	0.175	0.174
^{78}NI	0.287	0.285
^{88}SR	0.095	0.096
^{90}ZR	0.064	0.065
^{100}SN	-0.081	-0.078
^{132}SN	0.220	0.217
^{208}PB	0.160	0.155

TABLE XI: Single-particle energies (in MeV) for ^{40}Ca nucleus.

Orbits	Expt.	KDE0	KDE
Protons			
$1s_{1/2}$	-50 ± 11	-39.40	-38.21
$1p_{3/2}$	$-$	-26.95	-26.42
$1p_{1/2}$	-34 ± 6	-22.93	-22.34
$1d_{5/2}$	$-$	-14.49	-14.51
$2s_{1/2}$	-10.9	-9.48	-9.66
$1d_{3/2}$	-8.3	-7.59	-7.53
$1f_{7/2}$	-1.4	-2.38	-2.76
Neutrons			
$1s_{1/2}$	$-$	-47.77	-46.13
$1p_{3/2}$	$-$	-34.90	-33.92
$1p_{1/2}$	$-$	-30.78	-29.73
$1d_{5/2}$	$-$	-22.08	-21.66
$2s_{1/2}$	-18.1	-17.00	-16.78
$1d_{3/2}$	-15.6	-14.97	-14.48
$1f_{7/2}$	-8.32	-9.60	-9.58
$2p_{3/2}$	-6.2	-4.98	-5.15

TABLE XII: Single-particle energies (in MeV) for ^{208}Pb.

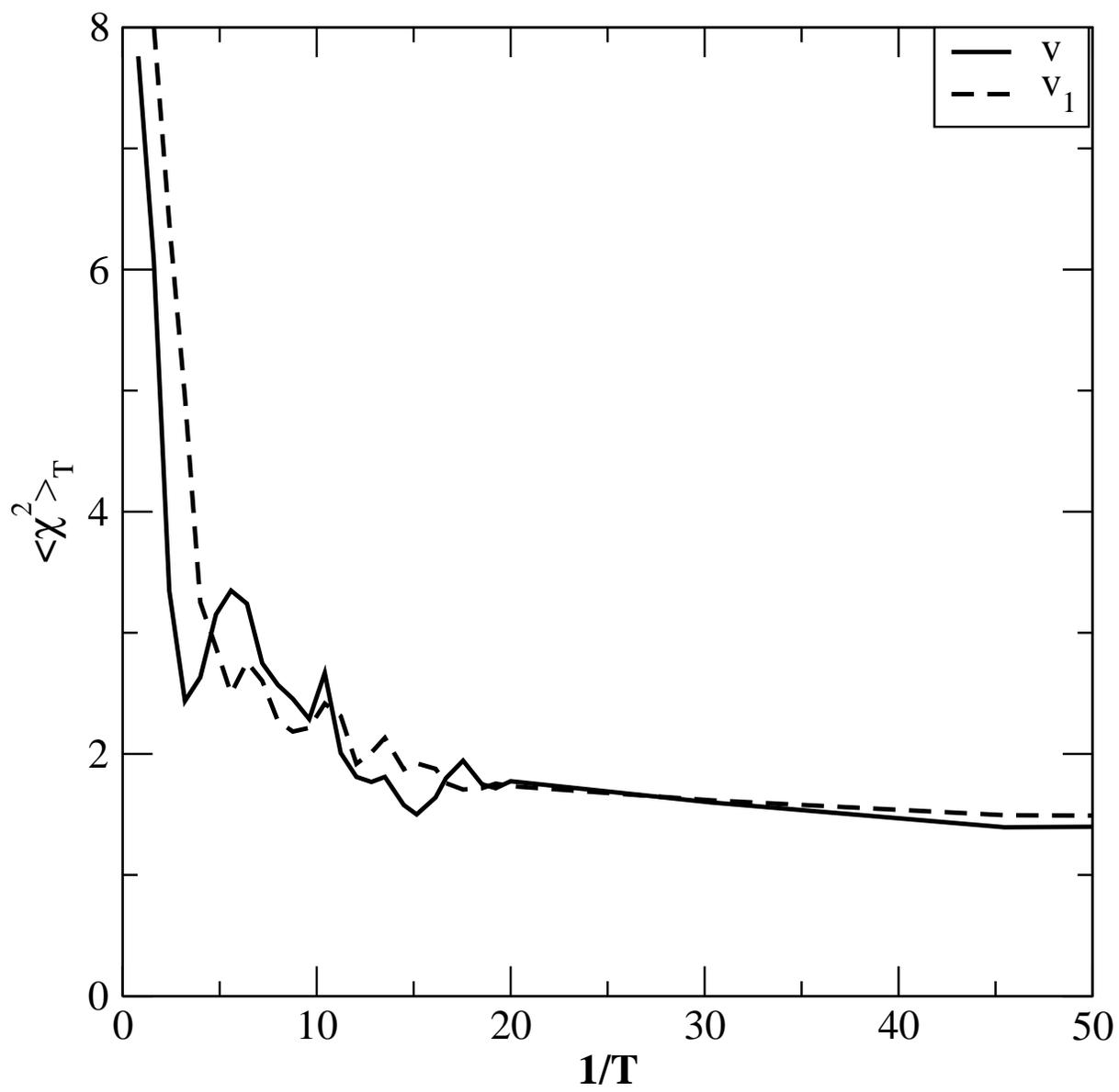| Orbits	Expt.	KDE0	KDE
Protons			
$1g_{9/2}$	−15.43	−17.85	−17.34
$1g_{7/2}$	−11.43	−13.77	−13.39
$2d_{5/2}$	−9.70	−11.37	−11.23
$1h_{11/2}$	−9.37	−9.87	−9.68
$2d_{3/2}$	−8.38	−9.43	−9.30
$3s_{1/2}$	−8.03	−8.67	−8.62
$1h_{9/2}$	−3.77	−4.00	−3.99
$2f_{7/2}$	−2.87	−2.78	−3.00
$1i_{13/2}$	−2.16	−1.62	−1.72
$3p_{3/2}$	−0.95	0.60	0.26
$2f_{5/2}$	−0.47	−0.19	−0.42
Neutrons			
$1h_{9/2}$	−10.85	−12.39	−12.24
$2f_{7/2}$	−9.72	−11.60	−11.64
$1i_{13/2}$	−9.01	−9.33	−9.20
$3p_{3/2}$	−8.27	−8.67	−8.77
$2f_{5/2}$	−7.95	−8.59	−8.64
$3p_{1/2}$	−7.38	−7.54	−7.65
$2g_{9/2}$	−3.94	−2.86	−3.06
$1i_{11/2}$	−3.15	−1.65	−1.69
$1j_{15/2}$	−2.53	−0.41	−0.43
$3d_{5/2}$	−2.36	−0.43	−0.64
$4s_{1/2}$	−1.91	0.08	−0.08
$2g_{7/2}$	−1.45	0.38	0.20
$3d_{3/2}$	−1.42	0.56	0.40

Fig. 1

Fig. 2

Fig. 3

Fig. 4